*chemistry*

MDPI

*Article*

# Solvent-Dependent Stabilization of Gold Nanoparticles: A Comparative Study on Polymers and the Influence of Their Molecular Weight in Water and Ethanol

**Marilyn Kaul [1], Rolf Lennart Vanselow [1], Ahmed Y. Sanin [2], Ulf D. Kahlert [2,3] and Christoph Janiak [1,*]**

[1] Institute for Inorganic and Structural Chemistry, Heinrich-Heine-University Düsseldorf, 40204 Düsseldorf, Germany; marilyn.kaul@uni-duesseldorf.de (M.K.); rvanselow@web.de (R.L.V.)
[2] Molecular and Experimental Surgery, University Clinic for General-, Visceral-, Vascular- and Transplant Surgery, Faculty of Medicine, Otto-von-Guericke-University Magdeburg, 39120 Magdeburg, Germany; ahmed.sanin@med.ovgu.de (A.Y.S.); ulf.kahlert@med.ovgu.de (U.D.K.)
[3] Research Campus Stimulate, Otto-von-Guericke-University Magdeburg, 39120 Magdeburg, Germany
* Correspondence: janiak@uni-duesseldorf.de; Tel.: +49-211-81-12286

**Abstract**

Gold nanoparticles (AuNPs) are attracting more and more attention in life sciences, especially due to their versatile physicochemical properties whereby their colloidal stability in water and organic solvents is crucial. In this study, a systematic comparison of different polymers, synthesis methods and solvents was carried out. The AuNPs were synthesized using the ligand exchange reaction/postsynthetic addition reaction (PAR) and the one-pot synthesis with the polymers poly(vinyl alcohol) (PVA), poly(ethylene glycol) (PEG), poly(vinylpyrrolidone) (PVP) and poly(acrylic acid) (PAA), each with different molar weight averages. Analysis of the AuNP@Polymer conjugates by transmission electron microscopy (TEM) finds essentially unchanged gold nanoparticle core sizes of 11–18 or 11–19 nm in water and ethanol, respectively. The hydrodynamic diameter from dynamic light scattering (DLS) lies largely in the range from 20 to 70 nm and ultraviolet-visible spectroscopy (UV-Vis) showed gold plasmon resonance band maxima between 517 and 531 nm over both synthesis methods and solvents for most samples. The polymer PVA showed the best colloidal stability in both synthesis methods, both in water and after transfer to ethanol. An increased instability in ethanol could only be noted for the PEG coated samples. For the polymers PVP and PAA, the stability depended more specifically on the combination of synthesis method, polymer molecular weight and solvent.

**Keywords:** gold nanoparticles; nanoparticle synthesis; polymer coating; stability; solvent

check for updates

Academic Editor: Huan Pang

Received: 11 August 2025
Revised: 16 September 2025
Accepted: 25 September 2025
Published: 1 October 2025

**Citation:** Kaul, M.; Vanselow, R.L.; Sanin, A.Y.; Kahlert, U.D.; Janiak, C. Solvent-Dependent Stabilization of Gold Nanoparticles: A Comparative Study on Polymers and the Influence of Their Molecular Weight in Water and Ethanol. *Chemistry* **2025**, *7*, 159. https://doi.org/10.3390/chemistry7050159

**Copyright:** © 2025 by the authors. Licensee MDPI, Basel, Switzerland. This article is an open access article distributed under the terms and conditions of the Creative Commons Attribution (CC BY) license (https://creativecommons.org/licenses/by/4.0/).

## 1. Introduction

Gold nanoparticles (AuNPs) are becoming increasingly popular due to their unique physical, chemical and optical properties and are being used more and more frequently in medicine, sensors, electronics or catalysis [1–3]. The synthesis of AuNPs is simple; they are biocompatible, air and water stable, the size and shape are easy to vary, they can be formulated with high solubility in water and they can be loaded with drugs or antibodies [4–7]. Due to their easy modification, AuNPs represent a versatile platform for a wide range of applications [8–10]. The targeted control of size, shape, monodispersity and surface functionalization of AuNPs plays a central role in their successful use in nanomedicine [11].

However, a key challenge and an important prerequisite for the application of AuNPs is to ensure that they are monodisperse and highly stable, especially when environmental

parameters like the solvent are changed. Therefore, polymers such as poly(vinyl alcohol) (PVA), poly(ethylene glycol) (PEG), poly(vinylpyrrolidone) (PVP) and poly(acrylic acid) (PAA) are applied as effective steric and electrostatic stabilizers [11] (Figure 1). The use of these polymers represents a promising approach for AuNP stabilization, as they form a protective shell around the AuNPs, minimizing particle-to-particle interactions and biofouling and increasing resistance to solvent changes [12–14]. The molecular weight of the polymers also plays a decisive role, as it significantly influences the density, thickness, and stability of the polymer shell and thus directly determines the stability of the AuNPs [15,16].

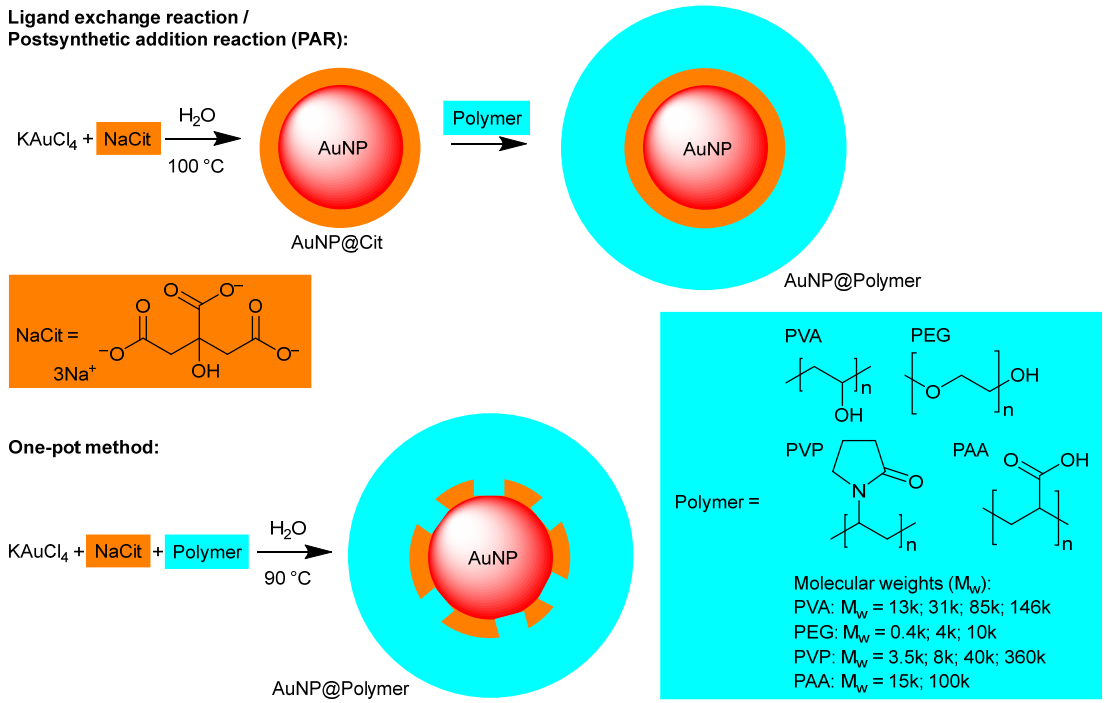


**Figure 1.** Schematic illustration of the AuNP synthesis methods and the polymers used for the AuNP@Polymer conjugates.

PEG is one of the most commonly used biopolymers for the steric stabilization of AuNPs in nanomedicine, which is also termed PEGylation [17,18]. PEG is thought to form a protective barrier around the nanoparticles to prevent their agglomeration, increase the biocompatibility of the AuNPs, prolong their circulation time in the blood, and to prevent them from being marked by the immune system and rapidly degraded [19–22]. According to reports, high-molecular-weight PEG (5000 Da)-coated AuNPs are more stable than low-molecular-weight PEG (2000 Da)-coated AuNPs in water [17]. A study has shown that AuNPs tend to agglomerate easily in the presence of low-molecular-weight PEG, whereas they remain stable with high-molecular-weight PEG even under extreme conditions, such as in organic solvent [23].

For certain biomedical applications, it is necessary for AuNPs to remain well-dispersed and stable in both water and organic solvents, such as ethanol [24]. A loss of stability and the subsequent associated aggregation usually lead to a loss of function of the AuNPs [25]. For example, some active pharmaceutical ingredients are only soluble in organic solvents and for their loading onto the AuNPs, the latter must be stable in the organic medium [26,27]. The active ingredient can be embedded in the polymer shell through supramolecular interactions with the polymers, which is advantageous as the chemical structure of the active ingredient remains unchanged, thus avoiding unexpected or unwanted reactions [11,28].

Various synthesis methods are often used to produce stabilized AuNPs [29,30], in particular, the ligand exchange reaction (termed here postsynthetic addition reaction, PAR) [31–33] and the one-pot method [34–36] (Figure 1). To our knowledge, however, the two approaches have not yet been systematically compared, especially with regard to the influence of the synthesis methods on the stability of the AuNPs using different polymers. A knowledge and comparison of different polymer-based stabilization and optimized synthesis methods are crucial to prepare stable AuNPs and to avoid unwanted agglomeration with loss of functionality [24,37]. As mentioned above, there are studies that have investigated the influence of the molecular weight of individual polymers on the stability of AuNPs [3,15,38], but there is no systematic comparison of different polymers with varying molecular weights. This was therefore the subject of our investigation.

For this purpose, different biocompatible polymers with varying molar weight averages and functional groups were applied to preformed Au-citrate nanoparticles. A thorough biological validation is outside the scope of this study.

## 2. Materials and Methods

### *2.1. Materials*

Potassium tetrachloridoaurate(III) ($KAuCl_4$), PVA $M_w$~13,000 g/mol, 31,000 g/mol, 85,000 g/mol, 146,000 g/mol, PEG $M_w$~400 g/mol, PVP $M_w$~3500 g/mol, 360,000, PAA $M_w$~15,000 g/mol and 100,000 were ordered from Sigma Aldrich, Darmstadt, Germany. PEG $M_w$~10,000 g/mol and PVP $M_w$~8000 g/mol were from Across Organics, Thermo Fisher Scientific, Schwerte, Germany. PEG $M_w$~4000 g/mol was purchased from JK Chemicals, Vapi, India and PVP $M_w$~40,000 g/mol was supplied from TCI, Eschborn, Germany. Sodium citrate dihydrate (NaCit) was from J.T. Baker Chemicals, Schwerte, Germany. Dasatinib (DASA) was obtained from BLD Pharmatech GmbH, Kaiserslautern, Germany. Ethanol with p.a. purity was obtained from Merck, Darmstadt, Germany.

Serum-free Dulbecco's modified Eagle medium and 30% F12 medium (DMEM/F12, Cat. Nr. 12634-028), B27 (Cat. Nr. 17504-044), GlutaMAX™ Supplement (Cat. Nr. 35050061), penicillin–streptomycin (Pen/Strep, Cat. 15140122) were purchased from Gibco™, Thermo Fisher Scientific, Schwerte, Germany. Human fibroblast growth factor-basic (FGF-2/bFGF, Cat. Nr. 100/18B), human epidermal growth factor (EGF, Cat. Nr. AF-100-15) were purchased from PeproTech®, Gibco™, ThermoFisher Scientific, Schwerte, Germany. Heparin (Cat. Nr. 194110) was procured from MP Biomed, Solon, OH, USA. The CellTiter-Glo 2.0 (Cat. G9242) cell viability glo kit was obtained from Promega, Madison, WI, USA.

All materials were commercially available and were used without further purification. Ultrapure water obtained from an Arium Mini® system from Sartorius (Sartorius AG, Göttingen, Germany) was used for the AuNPs synthesis.

### *2.2. Characterization Methods*

*Centrifuge:* The samples were centrifuge using the Sigma 3-30KHS from Sigma Laborzentrifugen GmbH (Sigma, Osterode am Harz, Germany). All centrifugation steps were performed at the specified parameters of the relative centrifugal force of 10,464× *g*, a time of 20 min, at a temperature of 4 °C, where g corresponds to the Earth's gravitational force. The relative centrifugal force (rcf) indicates the force acting on the sample as a multiple of the force of gravity.

*Transmission electron microscopy* (TEM): TEM images were recorded with a JEOL JEM-2100Plus electron microscope (JEOL, Tokyo, Japan) at an accelerating voltage of 200 kV with a Matataki Flash camera. The size of the AuNPs were measured with a GatanDigital Micrograph software (version 3.61) and over 200 particles were counted for the size distribution. Each AuNP solution was diluted by adding 20 µL of the AuNP sample to

either 80 µL of water, for the water samples, or 80 µL of ethanol, for the ethanol samples. 10 µL of the diluted dispersion was dropped onto a 200 µm carbon-coated copper grid from Electron Microscopy Sciences (Munich, Germany). The grid with the solution was dried at ambient conditions (~20 °C, ~50% relative humidity) and stored at ambient conditions in closed vials under air until the measurement.

*Dynamic light scattering* (DLS): Hydrodynamic diameters and the polydispersity index (PDI) were recorded with a Malvern Nano S Zetasizer (Malvern Panalytical, GmbH, Kassel, Germany) with a HeNe laser at a wavelength of 633 nm.

*Ultraviolet-visible* (UV-Vis): UV-Vis spectra were determined on a P9 double beam spectrophotometer (Radnor, PA, USA).

*High-performance liquid chromatography* (HPLC): The DASA concentration before and after loading was determined on a Shimadzu LC 20AT instrument (Shimadzu Corporation, Kyoto, Japan) with an SPD-M20A UV-Vis detector and a Luna C18(2) (250 × 4.60 mm, 5 micron) column from Phenomenex® (Aschaffenburg, Germany). The samples were filtered through a 0.2 µm Millex filter from Millipore® (Merck KGaA, Darmstadt, Germany) and all solvents used were degassed with the ultrasonic bath (Bandelin Sonorex, Berlin, Germany) before use. The mobile phase consisted of methanol–water (82:18, $v/v$) and had a flow-rate of 1 mL $min^{-1}$ at room temperature. The detector wavelength was set to 322 nm and the injection volume was 20 µL.

### *2.3. Synthesis of Polymer-Stabilized Gold Nanoparticles (AuNP@Polymer) in Water*

#### 2.3.1. Postsynthetic Addition Reaction

In a 500 mL Erlenmeyer flask with a glass stopper, a total of 20 mg (52.9 µmol) of $KAuCl_4$ was dispersed in 200 mL ultrapure water and heated to 100 °C. 90 mg (350 µmol) of NaCit was then added and the solution was heated to 100 °C for a further 15 min. During this time, the solution changed color from light yellow to dark red. Finally, the solution was cooled to room temperature, 4.3 µmol of polymer was added and stirring continued for 12 h. The DLS and UV-Vis measurements were taken directly after the 12 h. The DLS measurements were taken without dilution, and for the UV-Vis measurements, the solution was diluted with water in a ratio of 50:50. The remaining AuNP solutions were stored in the refrigerator at 4 °C in the reaction flask.

#### 2.3.2. One-Pot Synthesis

In a 500 mL round bottom flask, the amount of 20 mg (52.9 µmol) of $KAuCl_4$ and 4.3 µmol of polymer were dissolved in 200 mL of ultrapure water and the solution was heated to 90 °C under stirring. At 90 °C, 90 mg (350 µmol) of NaCit was added and the solution continued to be stirred for 30 min. The color changed from light yellow to dark red. The DLS and UV-Vis measurements were taken directly after cooling to room temperature and were measured as described in Section 2.3.1 above. The remaining AuNP solutions were stored in the refrigerator at 4 °C in the reaction flask.

### *2.4. Transfer of AuNP@Polymer from Water to Ethanol*

From the aqueous dispersion, 5 mL were centrifuged, the supernatant water was separated by decantation and discarded, and the AuNP@Polymer precipitate was resuspended in 5 mL of ethanol. The DLS and UV-Vis measurements were performed immediately afterwards. The solutions were measured in the DLS without dilution and the UV-Vis in a dilution of 50:50 (water:ethanol). The TEM grid and AuNP solutions storage were carried out as described above in Section 2.3.1.

### *2.5. Loading of DASA on the AuNP@Polymer Conjugates*

The AuNP@ conjugate samples were transferred from water to ethanol as described in Section 2.4. The 5 mL water or ethanol dispersion contains a gold mass mAu = 0.26 mg. From an ethanolic DASA stock solution (stored in refrigerator at 4 °C) with a concentration of 1 g/L, the volume of 0.8 mL (containing 0.8 mg DASA) was added to the 5 mL of the ethanolic AuNP@Polymer dispersion during stirring. The combined 5.8 mL of dispersion was stirred for further 72 h at ambient temperature. After 72 h the samples were centrifuged, and the supernatants were stored in the refrigerator at 4 °C until the HPLC measurement to determine the remaining DASA concentration in order to obtain the adsorbed amount on the AuNP@Polymer conjugate from the difference.

### *2.6. Cell Culture*

Four patient-derived glioblastoma stem cell (GSC) models were utilized in this study: GBM1, BTSC233, NCH421K and JHH520. GBM1, BTSC233, NCH421K and JHH520 cell models were provided by A. Vescovi, Stemgen S.p.A, Milan, Italy, C. Herold-Mende from the Department of Neurosurgery, Medical Center Heidelberg, Germany, Gregory J. Riggins, Baltimore, USA and M.S. Carro, Freiburg, Germany. Among these models, GBM1 represents the classical subtype, while BTSC233, NCH421K and JHH520 correspond to the mesenchymal subtype. Cells were maintained under serum-free conditions in a defined medium consisting of Dulbecco's modified Eagle medium (DMEM) supplemented with 30% F12, 2% B27, 20 ng/mL fibroblast growth factor (FGF), 20 ng $mL^{-1}$ epidermal growth factor (EGF), 5 µg $mL^{-1}$ heparin, 1% glutamine and 1% penicillin-streptomycin. To ensure cell line integrity and culture quality, short tandem repeat (STR) profiling was performed (Table S6) and mycoplasma contamination was excluded by PCR analysis following established protocols [27].

### *2.7. Growth Inhibition and Cell Viability Assay*

Cell seeding, viability assessment following drug exposure and statistical analyses of drug efficacy were performed according to the previously described method [27].

## 3. Results and Discussion

### *3.1. Synthesis and Characterization of the AuNP Samples in Water*

In this work, the ligand exchange reaction and the one-pot synthesis for the preparation of spherical AuNPs were investigated. In the two-step ligand exchange reaction, the AuNPs are first synthesized with citrate (from sodium citrate) which has the dual role of a reductant of the Au(III) precursor as well as a stabilizing agent. Then, in a second separate step another ligand or stabilizer is added to form the desired coating. Using this method, targeted surface modifications can be obtained and ligands can be used in the method that would not be suitable under the AuNP synthesis reaction conditions. However, it is unclear if the citrate anion coating on the gold surface is indeed replaced by neutral polymer chains or rather, if the polymer wraps around the citrate-stabilized AuNP particles (AuNP@Cit). In the classic Turkevich method, citrate acts as both a stabilizer and a reducing agent. It binds to the AuNP surface via its carboxylate groups. Through electrostatic interactions, citrate prevents the agglomeration of AuNPs. A polymer can interact with the AuNP surface in two different ways. If the polymer has functional groups with a strong affinity for gold, e.g., thiol groups in HS-PEG, the citrate molecules can be displaced from the AuNP surface [39–41]. If the polymer does not have a strong gold binding group, e.g., PEG, it attaches itself to the AuNP surface primarily via supramolecular interactions without forming a covalent bond. In this case, some of the citrate molecules remain on the AuNP surface, while the polymer forms an additional protective layer around the particles. In

most cases, however, a mixture of both types occurs, and it is for this reason that we will refer to a 'postsynthetic addition reaction' (PAR) instead of a 'ligand-exchange reaction' (Figure 1) [42,43]. In the single-step one-pot synthesis, the polymer is already present in the reaction mixture where the AuNPs are formed. Hence, the polymer coating can take place during the nucleation and growth steps in competition with citrate. This seems advantageous but can lead to competition between stabilization and growth, resulting in a larger variation in particle size [42,44–48].

In this work here we have started with citrate-stabilized AuNPs instead of 'uncoated' (or bare) AuNPs which are rarely produced in practice because they tend to agglomerate quickly. Furthermore, the production of such uncoated AuNPs requires a reduction in the gold precursor with $NaBH_4$, $SnCl_2$ or imidazolium ionic liquids instead of citrate which adds other reagents and renders a comparison to the citrate-polymer route difficult [49,50]. We note also that in the literature, 'uncoated' AuNPs are often used as a synonym for citrate-stabilized AuNPs [51,52].

The PAR consisted of first producing AuNP@Cit with the established Turkevich et al. method [53]. For this, $KAuCl_4$ was used as a gold precursor and sodium citrate as a reducing and stabilizing agent. Subsequently, the polymer was added to produce polymer-coated AuNPs. In the one-pot synthesis, the gold precursor ($KAuCl_4$), the reducing agent (NaCit) and the polymer were added to the reaction vessel.

The four following polymers with different molar weight averages were used here to compare the stability of the AuNPs: PVA with the molar masses ($M_W$) of 13,000; 31,000; 85,000 and 146,000 g/mol, PEG in the molar masses of 400; 4000 and 10,000 g/mol, PVP in the molar masses of 3500; 8000; 40,000 and 360,000 g/mol and PAA in the molar masses of 15,000 and 100,000 g/mol. The polymers with their molar masses are in the following designated from PVA13k, PVA146k, over PEG0.4k, PEG10k, PVP3.5k, PVP360k to PAA15k and PAA100k. The molar ratio of $KAuCl_4$ to polymer was always 12:1. This corresponded to a mass of 0.011 g of gold which was combined with polymer masses from 0.002 to 1.549 g, depending on the molecular weight of the polymer. These ratios were chosen based on a previous study in which they proved to be advantageous [27]. The masses of the polymers used are given in Table S2.

For characterization of the AuNP@Polymer conjugates, TEM provides a direct image of the gold cores of the conjugates with morphology, size, size distribution, dispersion or possible agglomeration, but does not visualize the size with the polymer. The TEM images of the AuNP@Polymer conjugates in water are shown in Figure 2 (PAR) and Figure 3 (one-pot), and Figure 4 provides a summarizing overview of the AuNP size. The corresponding size values are summarized in Table S1. The TEM images and the histograms in Figures 2 and 3 reveal with the PAR method spherical and monodisperse AuNP cores with an average size between 11 and 18 nm and a size-dispersion ($\sigma$) of mostly $\pm$1–2 nm (Table S1). In contrast, the one-pot method frequently produces anisotropic or elongated particles, particularly with the polymers PVP and PAA15k, where non-spherical and less stable AuNPs dominate. An exception is PAA100k, which yields unusually small spherical particles.

The comparison in Figure 4 illustrates that the one-pot synthesis gives largely a smaller average size of AuNPs than PAR. This may show a stabilizing effect of the polymer when present during the nucleation of the AuNP leading to a slower growth rate resulting in the formation of many small nuclei rather than a few large particles [54].

With the one-pot route and the polymers PVA, PVP and PAA, one can note that there are also smaller AuNPs formed with the longest polymer chains (highest molar mass). Polymers with a longer chain length increase the viscosity, which reduces the diffusion of

the gold ions in the dispersion, and this also slows down the growth rate which leads to smaller particles.

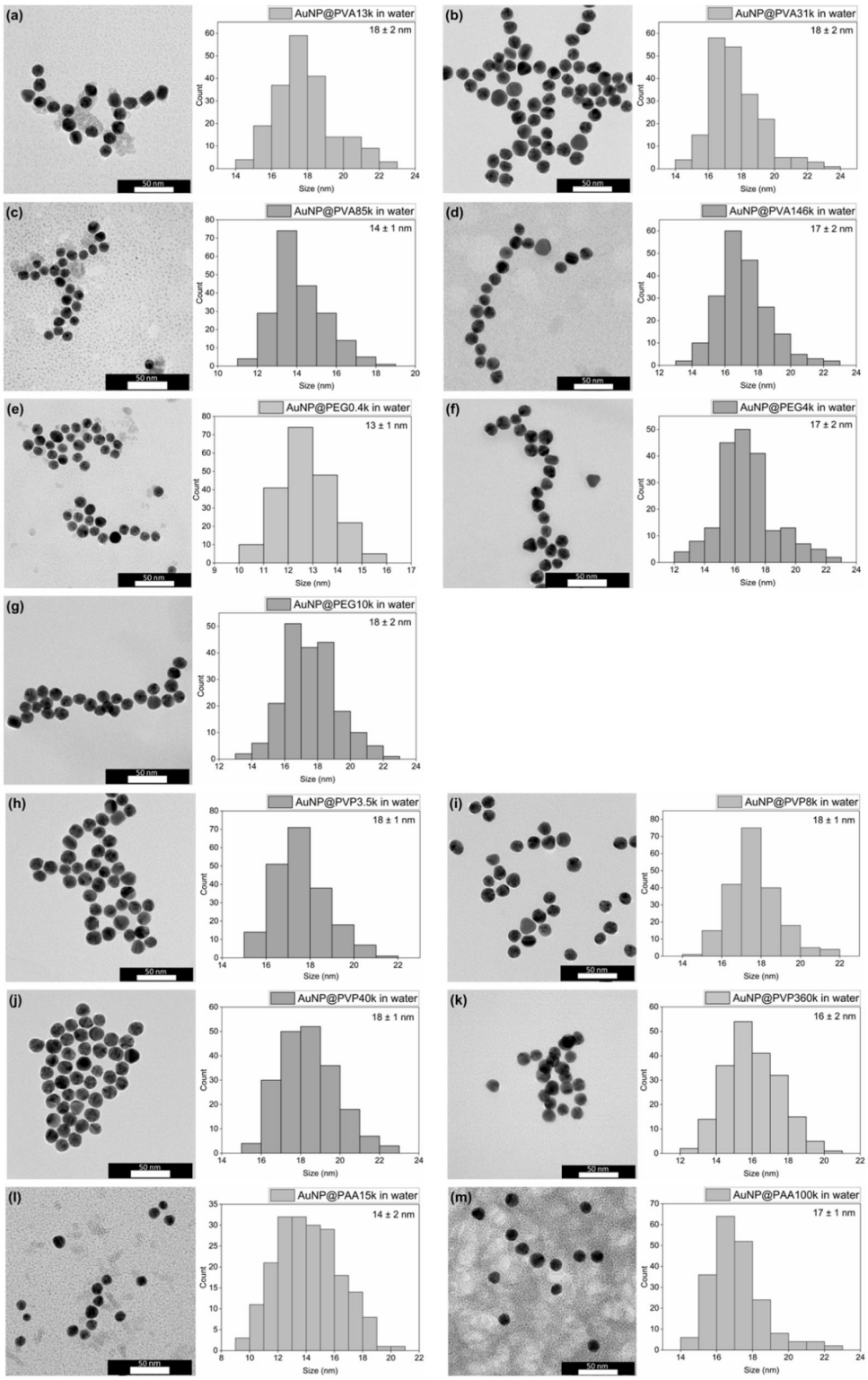


**Figure 2.** TEM images and histograms (with the average size and its standard deviation given) of the PAR synthesis in water of (**a**) AuNP@PVA13k, (**b**) AuNP@PVA31k, (**c**) AuNP@PVA85k, (**d**) AuNP@PVA146k, (**e**) AuNP@PEG0.4k, (**f**) AuNP@PEG4k, (**g**) AuNP@PEG10k, (**h**) AuNP@PVP3.5k, (**i**) AuNP@PVP8k, (**j**) AuNP@PVP40k, (**k**) AuNP@PVP360k, (**l**) AuNP@PAA15k and (**m**) AuNP@PAA100k. For the histograms, 200 particles were analyzed using larger areas of the TEM images. For the average size and standard deviation, see Table S1.

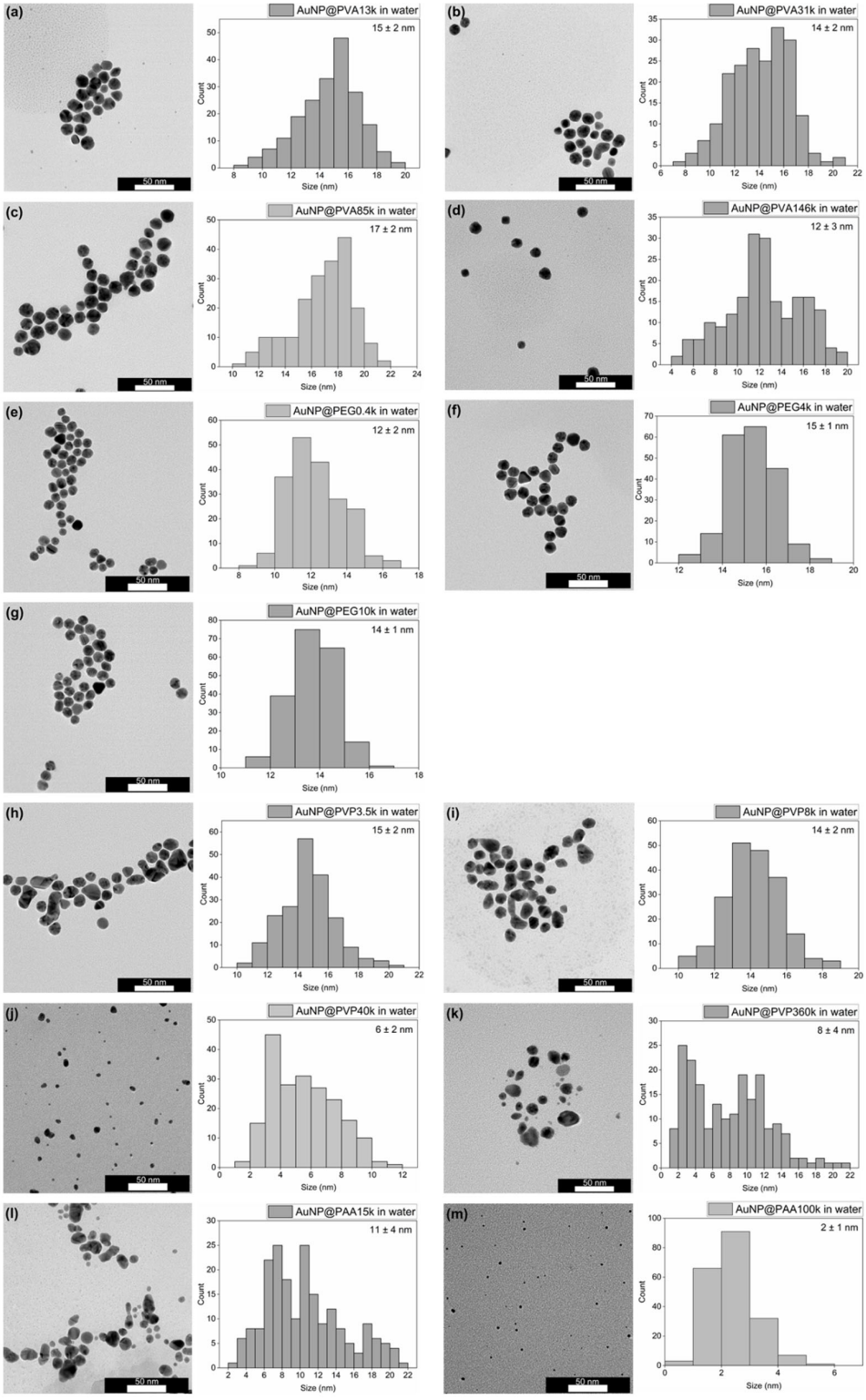


**Figure 3.** Representative TEM images and histograms (with the average size and its standard deviation given) of the one-pot synthesis in water of (**a**) AuNP@PVA13k, (**b**) AuNP@PVA31k, (**c**) AuNP@PVA85k, (**d**) AuNP@PVA146k, (**e**) AuNP@PEG0.4k, (**f**) AuNP@PEG4000, (**g**) AuNP@PEG10k, (**h**) AuNP@PVP3.5k, (**i**) AuNP@PVP8k, (**j**) AuNP@PVP40k, (**k**) AuNP@PVP360k, (**l**) AuNP@PAA15k and (**m**) AuNP@PAA100k. For the histograms, 200 particles were analyzed using larger areas of the TEM images. For the average size and standard deviation, see Table S1.

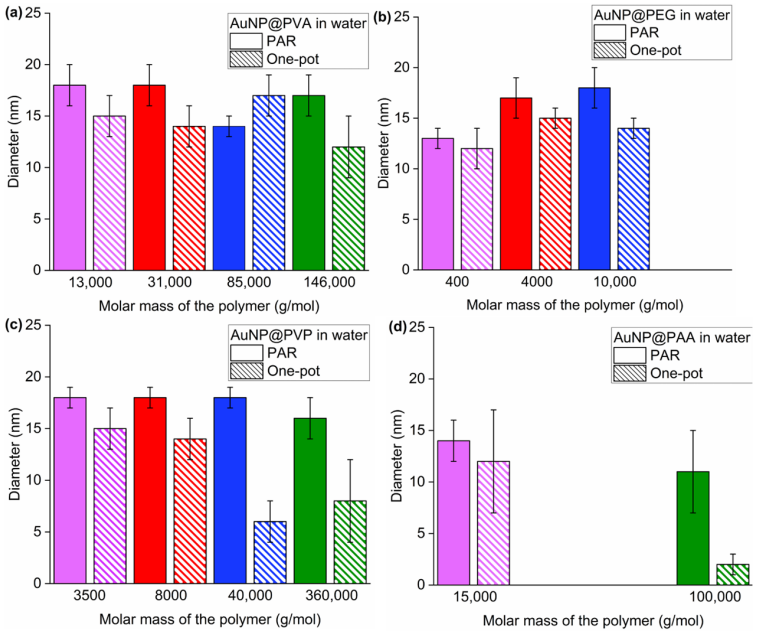


**Figure 4.** Overview of the TEM-derived AuNP core size and their standard deviation of the conjugates in water: (**a**) AuNP@PVA, (**b**) AuNP@PEG, (**c**) AuNP@PVP and (**d**) AuNP@PAA in water (fully colored bar PAR; hatched bar one-pot) (see also Table S1). The same color for different polymers simply indicates an increasing molecular weight; purple represents the polymer with the lowest molecular weight and green represents those with a molecular weight above 100,000 g/mol.

The gold core size dispersion for the two synthesis methods is also similar for PVA and PEG. Yet, with the polymers PVP and PAA, the size dispersion increases for the one-pot compared to the PAR synthesis. Interestingly, with PVP and PAA the one-pot synthesis also produced non-spherical AuNPs which are considered disadvantageous as non-spherical particles are usually less stable. Furthermore, spherical gold nanoparticles should be aimed for as non-spherical particles are more prone to agglomeration due to their curvature [12]. It is evident that the polymer functional groups, the chain length and mode of addition play a crucial role in determining the AuNP size, size dispersion and morphology.

For the synthesis of spherical AuNPs in water, the PAR method could successfully be used with all polymers and chain lengths. The one-pot method, on the other hand, only leads to the formation of spherical particles independent of chain lengths for the polymers PVA and PEG but not with PVP and PAA.

Direct and rapid size control of the dispersions is essential, and TEM measurements are time-consuming and require expensive instrumentation. Consequently, the samples were analyzed using DLS. The DLS gives the hydrodynamic diameter ($D_h$) and the polydispersity of the AuNPs, taking into account the polymer coating and the solvate shell due to the solvent, both of which cannot be determined by TEM. Due to the polymer and solvent shell, the DLS data generally show larger size values than the TEM data (see Figure 5 and Tables S1 and S3) [55,56]. From DLS, the heterogeneity of the sample is given by the PDI which is a dimensionless parameter for the width of the particle size distribution in a sample. It is derived from the analysis of the autocorrelation function in the DLS and provides information on the heterogeneity of the particle sizes. A PDI value below 0.05 is typically an indicator of a monomodal dispersion. Values between 0.10 and 0.25 are characteristic of a narrow distribution, while values above 0.50 indicate a significantly broader distribution. At values above 0.70, the system has a very broad size distribution, which is rather unsuitable for DLS measurements [57–59]. The hydrodynamic diameters from DLS of the polymer-stabilized AuNPs in the water are given in Table S1 (together with the TEM diameters and the UV-Vis bands) and the DLS diagrams are shown in Figures S2–S17.

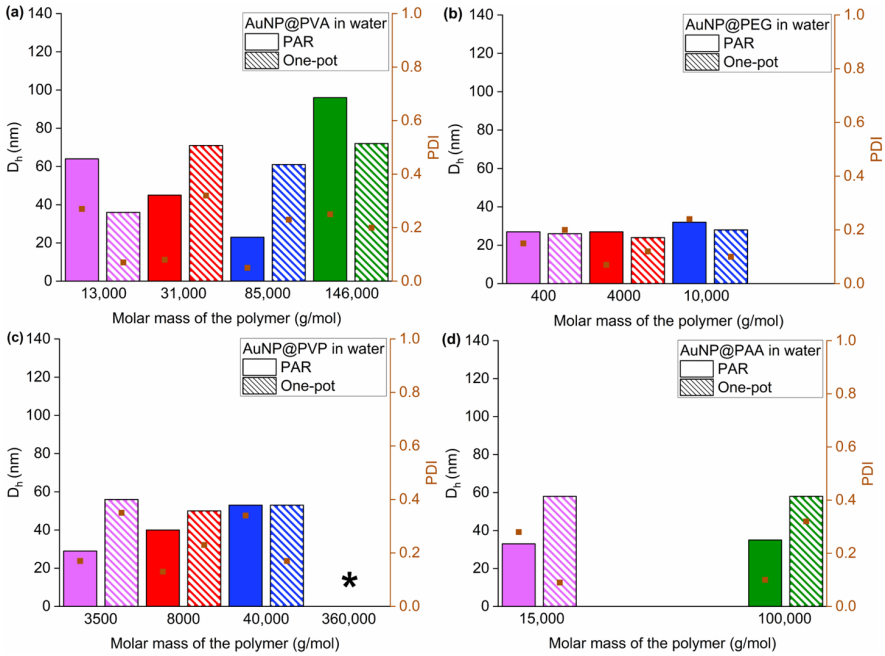


**Figure 5.** Graphical overview of all the DLS results in water of (**a**) AuNP@PVA, (**b**) AuNP@PEG, (**c**) AuNP@PVP and (**d**) AuNP@PAA (fully colored bar PAR; hatched bar one-pot). The brown squares represent the PDI. * The AuNP@PVP360k sample shows unexpectedly large hydrodynamic diameters for both the PAR method (177 nm) and the one-pot method (298 nm), which are off-scale (see also Table S1). The same color for different polymers simply indicates an increasing molecular weight; purple represents the polymer with the lowest molecular weight and green represents those with a molecular weight above 100,000 g/mol.

Figure 5 provides a summarized overview of the DLS results and shows that $D_h$ lies largely in the range of 20–70 nm for most samples, with the expected increase from the gold core size of 11–18 nm due to the polymer (and citrate) shell (Table S1). The one-pot method leads to a similar or higher $D_h$ compared to the PAR method. However, for the polymer PVA, the $D_h$ for the one-pot method also decreases for AuNP@PVA13k and AuNP@PVA146k compared to PAR. The $D_h$ values are generally very similar for the AuNP@PEG samples and the samples with PVP8k and PVP40k. The PEG-based AuNPs show a relative constant $D_h$, independent of the polymer molar mass. A higher $D_h$ by the one-pot method is then found for the AuNP conjugates with PVA31k and -85k, PVP3.5k and -360k and both PAA samples. The increase in $D_h$ seen for the PVP- and PAA-based AuNPs from the one-pot synthesis could be caused by the non-spherical morphology of the AuNP cores which was visible in the TEM images.

Non-spherical NPs can distort the results of the DLS measurements due to rotational movements and directional scattering, as the method is based on a spherical particle model. Anisotropic particles with different dimensions cannot be differentiated from each other in the DLS, as only an average hydrodynamic diameter is determined, which can deviate significantly from the actual particle dimensions. Although anisotropic particles may stand out in DLS due to a broad or multimodal size distribution, DLS does not provide accurate information about the particle shape [60]. It is again evident that the polymer functional groups, the chain length and mode of addition play a role in determining the AuNP@ conjugate size with its hydrodynamic diameter. The effect of increasing or decreasing $D_h$ does not only go in one direction when comparing the two synthesis methods of addition but also can reverse for a given polymer with its chain length. The interfacial interaction between the growing AuNPs, the citrate and polymer shell plays a decisive role, resulting in different and competing surface coverage during the AuNP formation and

growth. The general similarity of the hydrodynamic diameter of the PEG-based conjugates irrespective of polymer chain length which varies from 0.4k to 10k (in g/mol) may indicate little interaction of the PEG polymer with the AuNP@Cit surface. The more so as $D_h$ for AuNP@Cit is 25 nm, close to the $D_h$ values of 27, 27 and 32 nm for the three different AuNP@PEG conjugates (Table S1). This assumption of unperturbed AuNP@Cit particles in the presence of PEG is supported from their analysis in ethanol (see below).

While PEG is a very common polymer which is used for AuNPs in biosciences, it is not a polymer with high binding affinity to gold. However, cationic polymers or polymers with functional thiol, amine, or carboxyl groups have a higher binding affinity to gold [10]. The binding strength of coordinating groups to gold follows the order of S > P > N > O, meaning that amines and carboxylic acids form weaker bonds to gold than thiols and phosphines [61].

AuNPs exhibit a characteristic surface plasmon resonance (SPR), which typically occurs at around 520 nm for AuNPs synthesized with sodium citrate (NaCit) [62]. In colloidal form, this results in their reddish color. SPR is sensitive to various physicochemical parameters such as particle size, shape, environment and aggregation state, thereby enabling targeted control of optical properties. The aggregation of AuNPs leads to a shift in SPR and color change from red to blue, which can be used as a simple, visual indicator of instability or interactions in the solution [63]. As a test, we have used $NaBH_4$ for the reduction of $KAuCl_4$ and obtained intensely violet-colored solutions which thereby indicate larger AuNPs.

The UV-Vis data overview in Figure 6 for the PAR method and Figure S10 for the one-pot method shows very similar absorption maxima for the surface plasmon resonance in the range from 517 to 525 nm and similar band width for most samples in water (Table S1). The similarity in the absorption maxima and bandwidth reflects the similar size of the AuNP cores from TEM analysis in the range of 11–18 nm and with small size dispersion. An exception is the surface plasmon resonances (SPR) of the samples AuNP@PAA15k and AuNP@PAA100K from the one-pot method in water, with a significant red shift in the maximum to 533 nm which correlates with the polydispersity seen in the TEM sample.

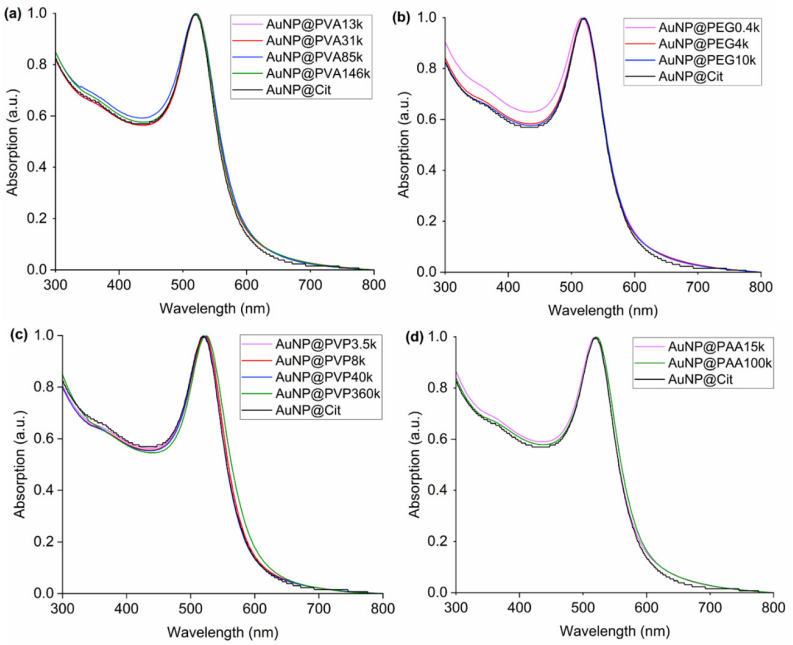


**Figure 6.** UV-Vis spectra in water from the PAR synthesis method of (**a**) AuNP@PVA, (**b**) AuNP@PEG, (**c**) AuNP@PVP and (**d**) AuNP@PAA. For the spectra from the one-pot method, see Figure S10. The absorption maxima are listed in Table S1.

### 3.2. Characterization of the AuNP Samples Transferred to Ethanol

The TEM analysis in Figures 7, S11 and S12 of the samples after their transfer into ethanol yields a range of 11–19 nm which is essentially identical to the 11–18 nm region of the samples in water (Table S1). The numerical data of all samples in ethanol are listed in Table S3. Small changes such as an increase in size by a few nanometers, for example, for PAR AuNP@PVA85k, AuNP@PEG0.4k and AuNP@PAA100k, for one-pot AuNP@PVA13k, AuNP@PVA146k, AuNP@PEG0.4k and AuNP@PEG10k (Figure 7) should not be overinterpreted as this deviation is still within the standard deviation of 3σ. However, the samples prepared by the one-pot method (Figure S14) with the polymers PVP and PAA100k, showed no longer well-separated, individual AuNPs. Instead, these samples depicted highly aggregated, anisotropic and non-spherical nanoparticles. The non-spherical nature of the AuNPs with PVP and PAA100k from the one-pot method was already observed in the TEM images in water, which were given in Figure 3, where the individual NPs could still be discerned. Due to this heterogeneous appearance, a reliable particle diameter analysis in ethanol based on the TEM images was not possible. It is evident that the polymers PVP and PAA in combination with the one-pot synthesis are less stabilizing for AuNPs, especially when the nanoparticles are transferred from water to ethanol.

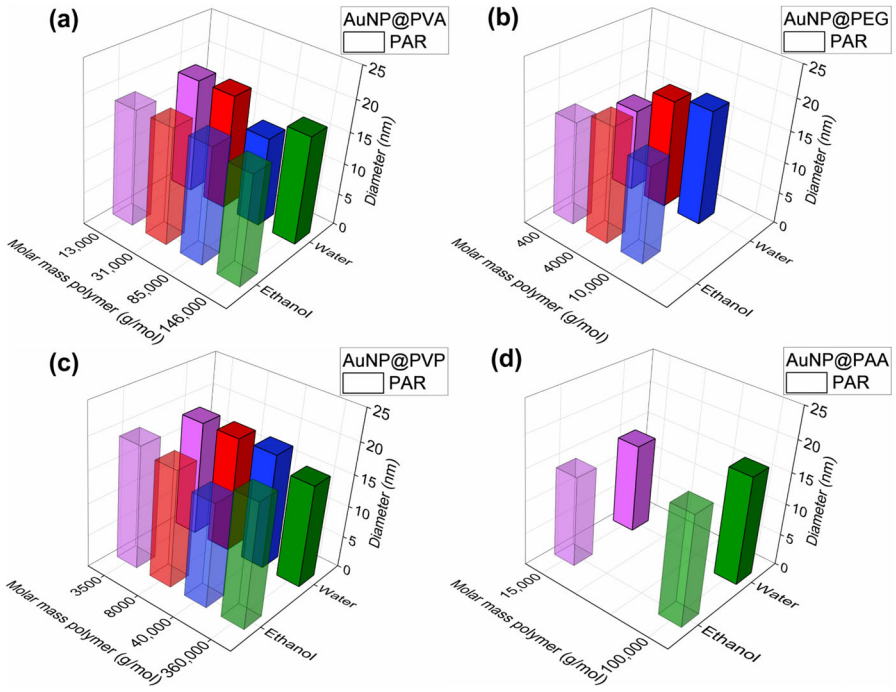


**Figure 7.** Comparative overview of the TEM size from PAR in water and ethanol of (**a**) AuNP@PVA, (**b**) AuNP@PEG, (**c**) AuNP@PVP and (**d**) AuNP@PAA. The individual TEM images for the ethanol samples are given in Figure S11, numerical data of the samples in ethanol is listed in Table S3. The bars for the ethanol dispersion are shown as transparent so that the bars in the water row can be seen more clearly. The same color for different polymers simply indicates an increasing molecular weight; purple represents the polymer with the lowest molecular weight and green represents those with a molecular weight above 100,000 g/mol.

The comparative overview of the hydrodynamic diameter from DLS from PAR in water and ethanol in Figure 8 indicates the expected increase in $D_h$ with increasing molar mass of the polymer. It can be concluded not only from TEM but also from DLS and UV-Vis (Figures 8, S23 and S25) that the nanoparticles from the PAR method remain rather unperturbed when transferred from water to ethanol. A single exception is the PEG10k-coated NPs. Here, DLS data in ethanol show a hydrodynamic diameter of 163 nm (vs.

32 nm in water) and a strong red-shift to 699 nm can be witnessed in the UV-Vis spectra (vs. 520 nm in water) (cf. Tables S1 and S3). Perhaps this aggregation deduced from the solution methods DLS and UV-Vis of the AuNP@PEG10k conjugates could also be inferred from the TEM image in Figure S11 where the individual gold cores are very close together, much closer than in the TEM images with the other polymers. This proximity where the nanoparticles appear to touch each other could derive from a missing polymer coating that was washed away. In the discussion of the DLS analysis in water, we had already noted that the very similar hydrodynamic diameter of the PEG-based conjugates, irrespective of polymer chain length, may indicate little interaction of the PEG polymer with the gold core, since PEG contains only ether groups that do not have a strong binding affinity to gold. Furthermore, nonpolar PEG provides a largely steric stabilization, whereas the more polar PVA, PVP and PAA polymers enable also some electrostatic stabilization. Further, the high solubility of PEG in ethanol also adds to its removal from the nanoparticle surface, leaving only the citrate layer, if any, and thus contributes to the tendency of the gold cores to aggregate [64–68].

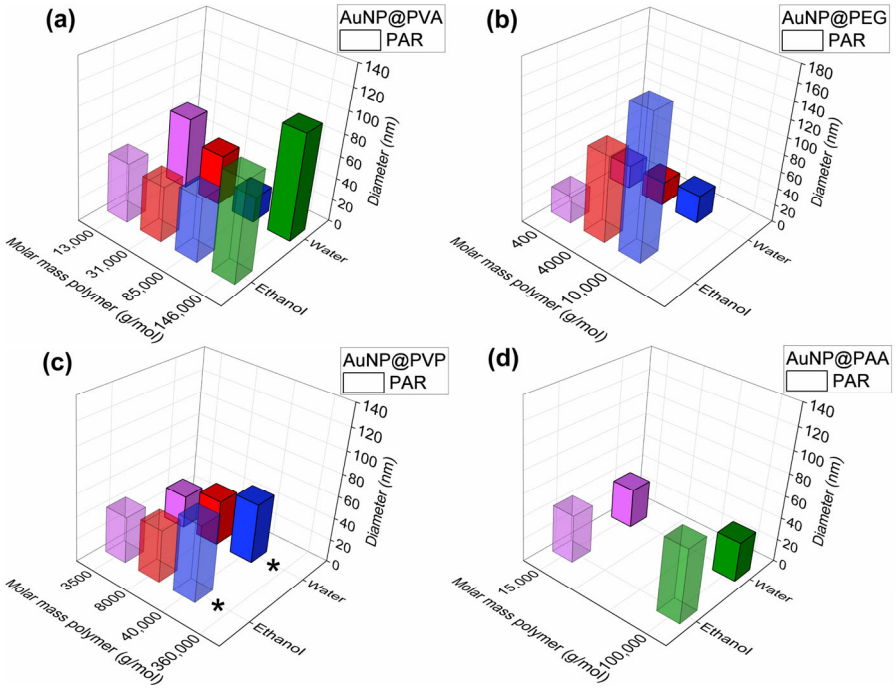


**Figure 8.** Comparative overview of the hydrodynamic diameter from DLS from PAR in water and ethanol of (**a**) AuNP@PVA, (**b**) AuNP@PEG, (**c**) AuNP@PVP and (**d**) AuNP@PAA. The individual DLS images for the ethanol samples are given in Figures S15–S18 and S23, numerical data of the samples in ethanol is listed in Table S3. The bars for the ethanol dispersion are shown transparent so that the bars in the water row can be seen more clearly. In ethanol some DLS values for PAR featured PDIs > 0.5 (AuNP@PEG10k, AuNP@PAA100k), which makes quantitative comparisons less reliable. * The AuNP@PVP360k samples show unexpectedly large hydrodynamic diameters (Tables S1 and S3), which are off-scale. The same color for different polymers simply indicates an increasing molecular weight; purple represents the polymer with the lowest molecular weight and green represents those with a molecular weight above 100,000 g/mol.

We note that aggregation here can mean two things: agglomeration of the gold nanoparticle cores or of the polymer shells surrounding two or more still separate AuNP cores, or a discrepancy between DLS and TEM will result when the polymer shells but not the AuNP cores aggregate. In TEM, only the still separate, albeit close, gold nanoparticle cores are seen whereas DLS detects the $(AuNP)_{2\text{-}3}$@Polymer conglomerate with its increased hydrodynamic diameter. Depending on the polymer, an opposite effect may

occur when the polymer is desorbed from the gold surface during sample dilution prior to the TEM measurement, thereby enabling AuNP core aggregation.

The nanoparticle instability from the one-pot synthesis (Figure S24) with the polymers PVP and PAA100k, which was evident in the TEM images (compare Figures 3 and S12), was not immediately evident in the DLS analysis of the PVP samples where the hydrodynamic diameter in ethanol remained similar to those measured in water (Figures 8, S23 and S24). Yet, in the UV-Vis spectra in ethanol, there is a broadening of the bands for AuNP@PVP, especially evident for PVP3.5k and PVP360k, also with a bathochromic shift to 531 nm and more significant to 576 nm for PVP360k (Figure S26, Table S3). From the one-pot synthesis, the longer-chain PEG conjugates exhibit a very large increase in hydrodynamic diameter in DLS after their transfer into ethanol (Figure 8). For UV-Vis and AuNP@PEG10k, the same strong red-shift as with PAR is seen in the one-pot product (Figures S25 and S26). For PAA100k, the hydrodynamic diameter increased in ethanol to 139 nm (vs. 58 nm in water) (cf. Tables S1 and S3) and the UV-Vis band strongly broadened (Figure S26).

For the AuNPs functionalized with PEG a tendency towards instability in ethanol can be inferred from the DLS and UV-Vis measurements similar to what observed in the case of PAR. Of all the polymers used in both synthesis methods, the PVA-coated AuNPs exhibit the highest colloidal stability both in water and after transfer to ethanol.

Overall, the AuNP@Polymer conjugates show less stabilization in ethanol than in water, also because highly polar water has a high dielectric constant (approx. 80), which gives stronger electrostatic interactions and can shield charges more efficiently. The dielectric constant of less polar ethanol is only about 25, which means that the electrostatic shielding is weaker, and the particles can attract each other and agglomerate [69,70]. Water also builds a stable hydrogen bond network to polymer chains with H-bond acceptors (OH in PVA, N-CO in PVP and $CO_2$- in PAA), which then can be solvated effectively. In ethanol, a weaker hydrogen bonding network is formed, so that the polymer shells of the AuNP@Polymer conjugates can approach and interact better, which results in their aggregation in solution [71–75].

To assess short-term stability, the AuNPs were suspended in ethanol for 3 days. The particle size determination by TEM shows no significant change for most samples after 3 days in ethanol (Figure S29, cf. Table S4 and Figure S13). However, despite the unchanged particle size, a clear agglomeration of the AuNP@PEG samples for both synthesis methods becomes evident (Figures S27 and S28). Further, the AuNP@PVP samples and AuNP@PAA100k from the one-pot method continued to show the highly aggregated, anisotropic and non-spherical nanoparticles as after the immediate TEM measurement (Figure S12).

### *3.3. Loading of DASA on the AuNP@Polymer Conjugates*

As a test for drug loading, we have investigated here the loading of the tyrosine kinase inhibitor (TKI) DASA (BMS-354825, Sprycel®), which required a change of the solvent to ethanol, as DASA is not soluble in water but in ethanol.

DASA (see Scheme S1 for the molecular structure) can be used as a drug to treat cancer and against drug resistance [76]. It inhibits the phosphorylation of the oncogenic and Src kinase families and can thus prevent angiogenesis and the associated tumor growth and support apoptosis [27,77,78]. As a TKI, it can be used in many tumor types such as leukemia, glioblastoma multiforme (GBM), pancreatic ductal adenocarcinoma (PDAC) and many others [79–82].

To determine the mass loading of DASA per mass of gold, the combined DASA and AuNP@Polymer dispersions (volume 5.8 mL) were stirred and centrifuged after 72 h. The supernatants were removed with a pipette and stored in the refrigerator at 4 °C until the HPLC measurement was performed. From the HPLC measurement, the remaining DASA

concentration was determined with the calibration curve in Figure S41. From the difference to the starting concentration of DASA the mass which was adsorbed on the AuNP@Polymer conjugate was obtained.

A typical DASA loading was in the range of 100–300 μg/mg of gold for all polymers except for PVA for both the PAR and one-pot method samples. For the PVA samples, the loading was consistently below 100 μg/mg and often close to no loading at all. This is because PVA has multiple hydroxyl groups and forms a stable hydrogen bond network with water in aqueous media, allowing it to swell in water. In ethanol, however, PVA has the lowest solubility of the polymers used here, which means that the H-bridge network with ethanol is significantly weaker [83–85]. This reduces the degree of swelling, causing the PVA polymer shell to adhere more densely and compactly to the AuNP surface, so that AuNP@PVA exhibit higher stability in ethanol than the conjugates with the other polymers, but this also means that the DASA molecules can only penetrate the polymer corona to a limited extent. There may be some correlation of the DASA loading for the PEG, PVP and PAA conjugates with their observed tendency of aggregation in ethanol as discussed above.

### *3.4. Growth Inhibition in Glioblastoma Stem Cell Models*

To evaluate whether AuNP@Polymer formulations could modulate the activity of DASA, we tested AuNPs, free DASA and DASA-loaded at AuNP@PVA31k across four glioblastoma stem cell (GSC) models, which represent both classical and mesenchymal molecular subtypes. As expected, AuNPs, that is, AuNP@PVA31k had negligible effects on cell viability, confirming the biocompatibility of the carrier system.

Treatment with DASA alone resulted in a time-dependent reduction in viability, with the most pronounced effect in NCH421K cells, where a significant decrease compared to control was observed by days 2 and 3 (Figure S42) at relatively high dose of 10 μmol $L^{-1}$. This indicates that certain GSC models retain partial sensitivity to Src-family kinase inhibition. In contrast, the remaining models (GBM1, BTSC233 and JHH520) displayed only modest viability reductions, in line with the heterogeneous and overall limited response profile of glioblastoma to DASA reported in preclinical and clinical studies [86].

When combined with AuNP@PVA31k, DASA induced growth inhibition patterns closely resembling those of free drug across all models. Importantly, activity was preserved after nanoparticle formulation, demonstrating that the drug remains bioactive after loading and release. However, no consistent potentiation of efficacy was observed compared with free DASA. This suggests that intrinsic resistance mechanisms in GSCs, such as the activation of compensatory pathways and efflux transporters like ABCB1/ABCG2 at the blood–brain barrier and at the cellular level likely dominate the therapeutic response [87].

Thus, our results confirm that DASA–AuNPs are stable, non-toxic carriers that preserve drug activity in vitro and reveal differential sensitivity among GSC models, with NCH421K showing the clearest response. The lack of marked improvement compared with DASA alone suggests that future work should focus on pairing AuNP delivery with compounds or drug combinations that have higher intrinsic potency in glioblastoma, thereby leveraging the delivery benefits of nanoparticles more effectively.

## 4. Conclusions

AuNP@Polymer conjugates were prepared in water by two different synthesis methods using polymers with different functional groups and chain lengths to compare their eligibility to stabilize the nanoparticles in water and ethanol. The gold precursor $KAuCl_4$ was reduced to Au(0) with sodium citrate. The polymers were either post-synthetically added (PAR) or were already present during the reduction in a one-pot method. Stable conjugates in water could be produced with all AuNP polymer systems using both PAR

and one-pot methods. Characterization by TEM and DLS yielded similar gold core sizes of 11–18 in water or 11–19 nm in ethanol, and hydrodynamic diameters of 20–70 nm for most AuNP@Polymer samples and both synthesis methods and solvents. Among all polymers tested (i) PVA is the most stable polymer in both water and ethanol, (ii) PEG shows poor stability in ethanol, (iii) PVP and PAA give solvent- and MW-dependent outcomes, (iv) DASA can be loaded successfully onto PEG, PVP, and PAA conjugates but not PVA and (v) PAR consistently yields spherical, stable particles across all polymers, while one-pot synthesis sometimes results in anisotropic or aggregated particles.

For future work, polymers with better coordinating groups such as thiol groups should be used, as gold has a high affinity for thiolated molecules; for example, Thio-PEG or Thio-PVA. These polymers bind to the AuNP surface via an S-linker and can enable a more stable polymer shell. Hydrophobic polymers such as poly(lactide-co-glycolide) could also be tested towards hydrophobic drug loading. Future works on the stabilizing effect of different polymers should also focus on the colloidal stability of AuNPs in complex biological media under physiologically relevant cell culture media conditions.

**Supplementary Materials:** The following supporting information can be downloaded at: https://www.mdpi.com/article/10.3390/chemistry7050159/s1, Section S1. Characterization of AuNP@Cit and AuNP@Polymer in water; Section S2.1. Characterization of AuNP@Polymer in ethanol after transfer from water; Section S2.2. Synthesis and characterization of the AuNP samples after 3 days in ethanol; Section S3. Quantification of DASA loading; Section S4. In vitro drug sensitivity test results. Section S5. References. References [88,89] are cited in the Supplementary Materials.

**Author Contributions:** Conceptualization, M.K., A.Y.S. and U.D.K.; methodology, M.K.; software, M.K.; validation, M.K.; formal analysis, M.K. and A.Y.S.; investigation, M.K., R.L.V. and A.Y.S.; resources, C.J.; data curation, M.K.; writing—original draft preparation, M.K.; writing—review and editing, M.K., A.Y.S., U.D.K. and C.J.; visualization, M.K.; supervision, C.J.; project administration, C.J.; funding acquisition, C.J. All authors have read and agreed to the published version of the manuscript.

**Funding:** Bundesamt für Strahlenschutz (FKZ 3622S7229B, Integrated molecular Imaging for Personalized Biomarker-based Breast Cancer Characterization and Treatment, IMMPRINT). This research has received funding from the European Union's EURATOM research and training programme under grant agreement No. 101061037 as part of the PIANOFORTE partnership. Further, the project was carried out with funds provided by the Federal Ministry for the Environment, Climate Action, Nature Conservation and Nuclear Safety (BMUKN) and on behalf of the Federal Office for Radiation Protection (BfS).

**Institutional Review Board Statement:** Not applicable.

**Informed Consent Statement:** Not applicable.

**Data Availability Statement:** The original contributions presented in this study are included in the article/Supplementary Materials. Further inquiries can be directed to the corresponding author.

**Acknowledgments:** The authors would like to thank the Core Facility for Electron Microscopy of the Institute of Medical Faculty of the Heinrich Heine University Düsseldorf for access to the JEOL JEM-2100Plus electron microscope instrument.

**Conflicts of Interest:** The authors declare no conflicts of interest.

## Abbreviations

The following abbreviations are used in this manuscript:

| | |
|---|---|
| AuNPs | Gold nanoparticles |
| PAR | Postsynthetic addition reaction |
| PVA | Poly(vinyl alcohol) |

| | |
|---|---|
| PEG | Poly(ethylene glycol) |
| PVP | Poly(vinyl pyrrolidone) |
| PAA | Poly(acrylic acid) |
| TEM | Transmission electron microscopy |
| UV-Vis | Ultraviolet-visible spectroscopy |
| DLS | Dynamic light scattering |
| HPLC | High-performance liquid chromatography |
| NaCit | Sodium citrate dihydrate |
| PDI | Polydispersity index |
| DASA | Dasatinib |
| GSC | Glioblastoma stem cells |

## References


1. Liang, M.; Lin, I.-C.; Whittaker, M.R.; Minchin, R.F.; Monteiro, M.J.; Toth, I. Cellular Uptake of Densely Packed Polymer Coatings on Gold Nanoparticles. *ACS Nano* **2010**, *4*, 403–413. [CrossRef]
2. Richards, S.-J.; Gibson, M.I. Optimization of the Polymer Coating for Glycosylated Gold Nanoparticle Biosensors to Ensure Stability and Rapid Optical Readouts. *ACS Macro Lett.* **2014**, *3*, 1004–1008. [CrossRef]
3. Wang, Y.; Quinsaat, J.E.Q.; Ono, T.; Maeki, M.; Tokeshi, M.; Isono, T.; Tajima, K.; Satoh, T.; Sato, S.-i.; Miura, Y.; et al. Enhanced dispersion stability of gold nanoparticles by the physisorption of cyclic poly(ethylene glycol). *Nat. Commun.* **2020**, *11*, 6089. [CrossRef]
4. Silva, V.C.J.D.; Silva, R.N.O.; Colli, L.G.; Carvalho, M.H.C.; Rodrigues, S.F. Gold nanoparticles carrying or not anti-VEGF antibody do not change glioblastoma multiforme tumor progression in mice. *Heliyon* **2020**, *6*, e05591. [CrossRef] [PubMed]
5. Kang, J.H.; Cho, J.; Ko, Y.T. Investigation on the effect of nanoparticle size on the blood-brain tumor barrier permeability by in situ perfusion via internal carotid artery in mice. *J. Drug Target.* **2018**, *27*, 103–110. [CrossRef]
6. Chen, Y.; Feng, X. Gold nanoparticles for skin drug delivery. *Int. J. Pharm.* **2022**, *625*, 122122. [CrossRef] [PubMed]
7. Nejati, K.; Dadashpour, M.; Gharibi, T.; Mellatyar, H.; Akbarzadeh, A. Biomedical Applications of Functionalized Gold Nanoparticles: A Review. *J. Clust. Sci.* **2022**, *33*, 1–16. [CrossRef]
8. Jain, P.K.; Lee, K.S.; El-Sayed, I.H.; El-Sayed, M.A. Calculated Absorption and Scattering Properties of Gold Nanoparticles of Different Size, Shape, and Composition: Applications in Biological Imaging and Biomedicine. *J. Phys. Chem. B* **2006**, *110*, 7238–7248. [CrossRef] [PubMed]
9. Huang, X.; El-Sayed, I.H.; Qian, W.; El-Sayed, M.A. Cancer Cell Imaging and Photothermal Therapy in the Near-Infrared Region by Using Gold Nanorods. *J. Am. Chem. Soc.* **2006**, *128*, 2115–2120. [CrossRef]
10. Siddique, S.; Chow, J.C.L. Gold Nanoparticles for Drug Delivery and Cancer Therapy. *Appl. Sci.* **2020**, *10*, 3824. [CrossRef]
11. Ghobashy, M.M.; Alkhursani, S.A.; Alqahtani, H.A.; El-damhougy, T.K.; Madani, M. Gold Nanoparticles in microelectronics advancements and biomedical applications. *Mater. Sci. Eng. B* **2024**, *301*, 117191. [CrossRef]
12. Sen, G.T.; Ozkemahli, G.; Shahbazi, R.; Erkekoglu, P.; Ulubayram, K.; Kocer-Gumusel, B. The Effects of Polymer Coating of Gold Nanoparticles on Oxidative Stress and DNA Damage. *Int. J. Toxicol.* **2020**, *39*, 328–340. [CrossRef]
13. Anniebell, S.; Gopinath, S.C.B. Polymer Conjugated Gold Nanoparticles in Biomedical Applications. *Curr. Med. Chem.* **2018**, *25*, 1433–1445. [CrossRef]
14. Hecold, M.; Buczkowska, R.; Mucha, A.; Grzesiak, J.; Rac-Rumijowska, O.; Teterycz, H.; Marycz, K. The Effect of PEI and PVP-Stabilized Gold Nanoparticles on Equine Platelets Activation: Potential Application in Equine Regenerative Medicine. *J. Nanomater.* **2017**, *1*, 8706921. [CrossRef]
15. Ling, K.; Jiang, H.; Zhang, Q. A colorimetric method for the molecular weight determination of polyethylene glycol using gold nanoparticles. *Nanoscale Res. Lett.* **2013**, *8*, 538. [CrossRef] [PubMed]
16. Seo, E.; Lee, S.-H.; Lee, S.; Choi, S.-H.; Hawker, C.J.; Kim, B.-S. Highly Stable Au Nanoparticles with Double Hydrophilic Block Copolymer Templates: Correlation between Structure and Stability. *Polym. Chem.* **2017**, *31*, 4528. [CrossRef]
17. Retout, M.; Blond, P.; Jabin, I.; Bruylants, G. Ultrastable PEGylated Calixarene-Coated Gold Nanoparticles with a Tunable Bioconjugation Density for Biosensing Applications. *Bioconjugate Chem.* **2021**, *32*, 290–300. [CrossRef] [PubMed]
18. Zhang, X.; Guo, X.; Kang, X.; Yang, H.; Guo, W.; Guan, L.; Wu, H.; Du, L. Surface Functionalization of Pegylated Gold Nanoparticles with Antioxidants Suppresses Nanoparticle-Induced Oxidative Stress and Neurotoxicity. *Chem. Res. Toxicol.* **2020**, *33*, 1195–1205. [CrossRef]
19. Kozics, K.; Sramkova, M.; Kopecka, K.; Begerova, P.; Manova, A.; Krivosikova, Z.; Sevcikova, Z.; Liskova, A.; Rollerova, E.; Dubaj, T.; et al. Pharmacokinetics, Biodistribution, and Biosafety of PEGylated Gold Nanoparticles In Vivo. *Nanomaterials* **2021**, *11*, 1702. [CrossRef]

20. Pedziwiatr-Werbicka, E.; Gorzkiewicz, M.; Horodecka, K.; Lach, D.; Barrios-Gumiel, A.; Sánchez-Nieves, J.; Gómez, R.; de la Mata, F.J.; Bryszewska, M. PEGylation of Dendronized Gold Nanoparticles Affects Their Interaction with Thrombin and siRNA. *J. Phys. Chem. B* **2021**, *125*, 1196–1206. [CrossRef]
21. Soares, S.; Faria, I.; Aires, F.; Monteiro, A.; Pinto, G.; Sales, M.G.; Correa-Duarte, M.A.; Guerreiro, S.G.; Fernandes, R. Application of Gold Nanoparticles as Radiosensitizer for Metastatic Prostate Cancer Cell Lines. *Int. J. Mol. Sci.* **2023**, *24*, 4122. [CrossRef]
22. Nguyenova, H.Y.; Kalbacova, M.H.; Dendisova, M.; Sikorova, M.; Jarolimkova, J.; Kolska, Z.; Ulrychova, L.; Weber, J.; Reznickova, A. Stability and biological response of PEGylated gold nanoparticles. *Heliyon* **2024**, *10*, e30601. [CrossRef]
23. Lee, J.W.; Choi, S.-R.; Heo, J.H. Simultaneous Stabilization and Functionalization of Gold Nanoparticles via Biomolecule Conjugation: Progress and Perspectives. *ACS Appl. Mater. Interfaces* **2021**, *13*, 42311–42328. [CrossRef]
24. Tsutsui, G.; Huang, S.; Sakaue, H.; Shingubara, S.; Takahagi, T. Well-size-controlled Colloidal Gold Nanoparticles Dispersed in Organic Solvents. *Jpn. J. Appl. Phys.* **2001**, *40*, 346–349. [CrossRef]
25. Hussain, M.H.; Abu Bakar, N.F.; Mustapa, A.N.; Low, K.-F.; Othman, N.H.; Adam, F. Synthesis of Various Size Gold Nanoparticles by Chemical Reduction Method with Different Solvent Polarity. *Nanoscale Res. Lett.* **2020**, *15*, 140. [CrossRef]
26. Aboudzadeh, M.A.; Kruse, J.; Iglesias, M.S.; Cangialosi, D.; Alegria, A.; Grzelczak, M.; Barroso-Bujans, F. Gold nanoparticles endowed with low-temperature colloidal stability by cyclic polyethylene glycol in ethanol. *Soft Matter* **2021**, *17*, 7792–7801. [CrossRef]
27. Kaul, M.; Sanin, A.Y.; Shi, W.; Janiak, C.; Kahlert, U.D. Nanoformulation of dasatinib cannot overcome therapy resistance of pancreatic cancer cells with low LYN kinase expression. *Pharmacol. Rep.* **2024**, *76*, 793–806. [CrossRef] [PubMed]
28. Giesen, B.; Nickel, A.-C.; Barthel, J.; Kahlert, U.D.; Janiak, C. Augmented Therapeutic Potential of Glutaminase Inhibitor CB839 in Glioblastoma Stem Cells Using Gold Nanoparticle Delivery. *Pharmaceutics* **2021**, *13*, 295. [CrossRef]
29. Vinnacombe-Willson, G.A.; Conti, Y.; Stefancu, A.; Weiss, P.S.; Cortés, E.; Scarabelli, L. Direct Bottom-Up In Situ Growth: A Paradigm Shift for Studies in Wet-Chemical Synthesis of Gold Nanoparticles. *Chem. Rev.* **2023**, *123*, 8488–8529. [CrossRef] [PubMed]
30. Guyot, C.; Leclère, P.; Voué, M. Gold nanoparticles growing in a polymer matrix: What can we learn from spectroscopic imaging ellipsometry? *J. Vac. Sci. Technol. B* **2020**, *38*, 013602. [CrossRef]
31. Maleeva, K.; Pavllova, A.; Samofalov, G.; Baranov, M.; Smirnov, E.; Bogdanov, K. Easily fabricated SERS tags based on spherical polymer matrices decorated by gold nanoparticles. *J. Phys. Conf. Ser.* **2025**, *2978*, 012003. [CrossRef]
32. Duan, H.; Luo, Q.; Wie, Z.; Lin, Y.; He, J. Symmetry-Broken Patches on Gold Nanoparticles through Deficient Ligand Exchange. *ACS Macro Lett.* **2021**, *10*, 786–790. [CrossRef] [PubMed]
33. Hočevar, S.; Milošević, A.; Rodriguez-Lorenzo, L.; Ackermann-Hirschi, L.; Mottas, I.; Petri-Fink, A.; Rothen-Rutishauser, B.; Bourquin, C.; Clift, M.J.D. Polymer-Coated Gold Nanospheres Do Not Impair the Innate Immune Function of Human B Lymphocytes in Vitro. *ACS Nano* **2019**, *13*, 6790–6800. [CrossRef]
34. Wen, C.; Broholm, M.M.; Dong, J.; Uthuppu, B.; Jakobsen, M.H.; Fjordbøge, A.S. Transport of citrate and polymer coated gold nanoparticles (AuNPs) in porous media: Effect of surface property and Darcy velocity. *J. Environ. Sci.* **2020**, *92*, 235–244. [CrossRef]
35. Mondo, G.B.; da Silva Ribeiro, C.A.; Schlüter, L.G.; Bellettini, I.C.; Pavlova, E.; Giacomelli, F.C. One-Pot Bottom-up Synthesis of Gold Nanoparticles Mediated by Nitrogen-Containing Polymers: The Role of Chain Features and Environmental Conditions. *Colloids Surf. A Physicochem. Eng. Asp.* **2024**, *703*, 135116. [CrossRef]
36. Ribeiro, C.A.S.; Albuquerque, L.J.C.; de Castro, C.E.; Pereira, R.M.; Albuquerque, B.L.; Pavlova, E.; Schlüter, L.G.; Batista, B.L.; Bellettini, I.C.; Giacomelli, F.C. Ready-to-use room temperature one-pot synthesis of surface-decorated gold nanoparticles with targeting attributes. *J. Colloid Interface Sci.* **2022**, *614*, 489–501. [CrossRef]
37. Reznickova, A.; Slepicka, P.; Slavikova, N.; Staszek, M.; Svorcik, V. Preparation, aging and temperature stability of PEGylated gold nanoparticles. *Colloids Surf. A* **2017**, *523*, 91–97. [CrossRef]
38. Brough, C.; Miller, D.A.; Keen, J.M.; Kucera, S.A.; Lubda, D.; Williams, R.O., III. Use of Polyvinyl Alcohol as a Solubility-Enhancing Polymer for Poorly Water Soluble Drug Delivery (Part 1). *AAPS PharmSciTech* **2016**, *17*, 167–179. [CrossRef]
39. Li, J.; Zhu, B.; Yao, X.; Zhang, Y.; Zhu, Z.; Tu, S.; Jia, S.; Liu, R.; Kang, H.; Yang, C.J. Synergetic Approach for Simple and Rapid Conjugation of Gold Nanoparticles with Oligonucleotides. *ACS Appl. Mater. Interfaces* **2014**, *6*, 16800–16807. [CrossRef] [PubMed]
40. Meesaragandla, B.; García, I.; Biedenweg, D.; Toro-Mendoza, J.; Coluzza, I.; Liz-Marzán, L.M.; Delcea, M. H-Bonding-Mediated Binding and Charge Reorganization of Proteins on Gold Nanoparticles. *Phys. Chem. Chem. Phys.* **2020**, *22*, 4490–4500. [CrossRef] [PubMed]
41. Weisbecker, C.S.; Merritt, M.V.; Whitesides, G.M. Molecular Self-Assembly of Aliphatic Thiols on Gold Colloids. *Langmuir* **1996**, *12*, 3763–3772. [CrossRef]
42. Thambiliyagodage, C. Ligand exchange reactions and PEG stabilization of gold nanoparticles. *Curr. Res. Green Sustain. Chem.* **2022**, *5*, 100245. [CrossRef]
43. Singh, R.; Srinivas, S.P.; Kumawat, M.; Daima, H.K. Ligand-based surface engineering of nanomaterials: Trends, challenges, and biomedical perspectives. *OpenNano* **2024**, *15*, 100194. [CrossRef]

44. Le Goas, M.; Saber, J.; Bolívar, S.G.; Rabanel, J.-M.; Awogni, J.-M.; Boffito, D.C.; Banquy, X. (In)stability of ligands at the surface of inorganic nanoparticles: A forgotten question in nanomedicine? *Nano Today* **2022**, *45*, 101516. [CrossRef]
45. Woehrle, G.H.; Brown, L.O.; Hutchison, J.E. Thiol-Functionalized, 1.5-nm Gold Nanoparticles through Ligand Exchange Reactions: Scope and Mechanism of Ligand Exchange. *J. Am. Chem. Soc.* **2005**, *127*, 2172–2183. [CrossRef]
46. Ishida, Y.; Suzuki, J.; Akita, I.; Yonezawa, T. Ultrarapid Cationization of Gold Nanoparticles via a Single-Step Ligand Exchange Reaction. *Langmuir* **2018**, *34*, 10668–10672. [CrossRef]
47. Fan, B.; Liu, Y.; Wan, J.; Crawford, S.; Thang, S.H. Polymerization-Induced Self-Assembly (PISA) and "Host–Guest" Complexation-Directed Polymer/Gold Nanocomposites. *ACS Mater. Lett.* **2020**, *2*, 492–498. [CrossRef]
48. Young, H.L.; McCormick, C.R.; Butterfield, A.G.; Gomez, E.D.; Schaak, R.E. Postsynthetic Thiol-Induced Reshaping of Copper Sulfide Nanoparticles. *Chem. Mater.* **2022**, *34*, 11014–11025. [CrossRef]
49. Redel, E.; Walter, M.; Thomann, R.; Vollmer, C.; Hussein, L.; Scherer, H.; Krüger, M.; Janiak, C. Synthesis, stabilization, functionalization and DFT calculations of gold nanoparticles in fluorous phases (PTFE and ILs). *Chem. Eur. J.* **2009**, *15*, 10047–10059. [CrossRef] [PubMed]
50. Redel, E.; Walter, M.; Thomann, R.; Hussein, L.; Krüger, M.; Janiak, C. Stop-and-go, stepwise and "ligand-free" nucleation, nanocrystal growth and formation of Au-NPs in ionic liquids (ILs). *Chem. Commun.* **2010**, *46*, 1159–1161. [CrossRef] [PubMed]
51. Albertini, B.; Mathieu, V.; Iraci, N.; Van Woensel, M.; Schoubben, A.; Donnadio, A.; Greco, S.M.; Ricci, M.; Temperini, A.; Blasi, P.; et al. Tumor Targeting by Peptide-Decorated Gold Nanoparticles. *Mol. Pharm.* **2019**, *16*, 2430–2444. [CrossRef]
52. Alobaid, M.A.; Richards, S.-J.; Alexander, M.R.; Gibson, M.I. Ghaemmaghami. Monosaccharide coating modulate the intracellular trafficking of gold nanoparticles in dendritic cells. *Mater. Today Bio* **2024**, *29*, 101371. [CrossRef]
53. Turkevich, J.; Stevenson, P.C.; Hillier, J. A study of the nucleation and growth processes in the synthesis of colloidal gold. *Discuss. Faraday Soc.* **1951**, *11*, 55–75. [CrossRef]
54. Shimmin, R.G.; Schoch, A.-B.; Braun, P.V. Polymer Size and Concentration Effects on the Size of Gold Nanoparticles Capped by polymeric Thiols. *Langmuir* **2004**, *20*, 5613–5620. [CrossRef] [PubMed]
55. Leoncini, M.; Ortile, C.; Tinello, S.; Gross, S.; Mognato, M. Comparative cytotoxicity of biogenic and chemical silver and gold nanoparticles on normal and tumoral lung cells. *J. Drug Deliv. Sci. Technol.* **2025**, *113*, 107335. [CrossRef]
56. Mahapatra, S.D.; Bhattacharya, D.; Das, S.; Mandal, S.; Sen, N.; Sepay, N.; Bhattacharya, S.K.; Ghosh, A.; Sinha, C. Allium Sativum Manipulated AgNP-Metformin Conjugated Nanostructure: Therapeutic Strategy for Enhanced Antibacterial Action against Multidrug-Resistant *Staphylococcus aureus* and *Escherichia coli*. *ChemistrySelect* **2025**, *10*, e01282. [CrossRef]
57. Gharib, R.; Greige-Gerges, H.; Fourmentin, S.; Charcosset, C. Hydroxypropyl-ß-cyclodextrin as a membrane protectant during freeze-drying of hydrogenated and non-hydrogenated liposomes and molecule-in-cyclodextrin-in- liposomes: Application to trans-anethole. *Food Chem.* **2018**, *267*, 67–74. [CrossRef]
58. Danaei, M.; Dehghankhold, M.; Ataei, S.; Hasanzadeh Davarani, F.; Javanmard, R.; Dokhani, A.; Khorasani, S.; Mozafari, M.R. Impact of Particle Size and Polydispersity Index on the Clinical Applications of Lipidic Nanocarrier Systems. *Pharmaceutics* **2018**, *10*, 57. [CrossRef]
59. Hoseini, B.; Jaafari, M.R.; Golabpour, A.; Momtazi-Borojeni, A.A.; Karimi, M.; Eslami, S. Application of ensemble machine learning approach to assess the factors affecting size and polydispersity index of liposomal nanoparticles. *Sci. Rep.* **2023**, *13*, 18012. [CrossRef] [PubMed]
60. Feller, D.; Otten, M.; Hildebrandt, M.; Krüsmann, M.; Bryant, G.; Karg, M. Translational and rotational diffusion coefficients of gold nanorods functionalized with a high molecular weight, thermoresponsive ligand: A depolarized dynamic light scattering study. *Soft Matter* **2021**, *17*, 4019. [CrossRef]
61. Raji, F.; Peng, Y. Review of gold-ligand interactions: Implications for metallurgical processes and nanoparticle synthesis. *Adv. Colloid Interface Sci.* **2025**, *345*, 103644. [CrossRef]
62. Sani, A.; Cao, C.; Cui, D. Toxicity of gold nanoparticles (AuNPs): A review. *Biochem. Biophys. Rep.* **2021**, *26*, 100991. [CrossRef] [PubMed]
63. Kesharwani, P.; Ma, R.; Sang, L.; Fatima, M.; Sheikh, A.; Abourehab, M.A.S.; Gupta, N.; Chen, Z.-S.; Zhou, Y. Gold nanoparticles and gold nanorods in the landscape of cancer therapy. *Mol. Cancer* **2023**, *22*, 98. [CrossRef] [PubMed]
64. Zhang, X.; Jimmy Huang, P.-J.; Servos, M.R.; Liu, J. Effects of Polyethylene Glycol on DNA Adsorption and Hybridization on Gold Nanoparticles and Graphene Oxide. *Langmuir* **2012**, *28*, 14330–14337. [CrossRef] [PubMed]
65. Uz, M.; Bulmus, V.; Altinkaya, S.A. Effect of PEG Grafting Density and Hydrodynamic Volume on Gold Nanoparticle–Cell Interactions: An Investigation on Cell Cycle, Apoptosis, and DNA Damage. *Langmuir* **2016**, *32*, 5997–6009. [CrossRef] [PubMed]
66. Chen, H.; Paholak, H.; Ito, M.; Sansanaphongpricha, K.; Qian, W.; Che, Y.; Sun, D. 'Living' PEGylation on gold nanoparticles to optimize cancer cell uptake by controlling targeting ligand and charge densities. *Nanotechnology* **2013**, *24*, 355101. [CrossRef]
67. Aboudzadeh, M.A.; Iturrospe, A.; Arbe, A.; Grzelczak, M.; Barroso-Bujans, F. Cyclic Polyethylene Glycol as Nanoparticle Surface Ligand. *ACS Macro Lett.* **2020**, *9*, 1604–1610. [CrossRef]
68. Paul, D.; Ganesan, R.; Ray Dutta, J. Effect of polymeric additives on gold nanoparticles for colorimetric detection of hepatitis C virus. *Gold Bull.* **2025**, *58*, 8. [CrossRef]

69. Mohsen-Nia, M.; Amiri, H.; Jazi, B. Dielectric Constants of Water, Methanol, Ethanol, Butanol and Acetone: Measurement and Computational Study. *J. Solut. Chem.* **2010**, *39*, 701–708. [CrossRef]
70. Tseng, K.-H.; Liao, C.-Y.; Huang, J.-C.; Tien, D.-C.; Tsung, T.-T. Characterization of gold nanoparticles in organic or inorganic medium (ethanol/water) fabricated by spark discharge method. *Mater. Lett.* **2008**, *62*, 3341–3344. [CrossRef]
71. Liao, J.; Zhang, Y.; Yu, W.; Xu, L.; Ge, C.; Liu, J.; Gu, N. Linear aggregation of gold nanoparticles in ethanol. *Colloids Surf. A Physicochem. Eng. Asp.* **2003**, *223*, 177–183. [CrossRef]
72. Tilaki, R.M.; Iraji zad, A.; Mahdavi, S.M. The effect of liquid environment on size and aggregation of gold nanoparticles prepared by pulsed laser ablation. *J. Nanopart. Res.* **2007**, *9*, 853–860. [CrossRef]
73. Lu, H.; Huang, W.M.; Fu, Y.Q.; Leng, J. Quantitative separation of the influence of hydrogen bonding of ethanol-water mixture on the shape recovery behavior of polyurethane shape memory polymer. *Smart Mater. Struct.* **2014**, *23*, 125041. [CrossRef]
74. Jewrajka, S.K.; Chatterjee, U. Block copolymer mediated synthesis of amphiphilic gold nanoparticles in water and an aqueous tetrahydrofuran medium: An approach for the preparation of polymer–gold nanocomposites. *J. Polym. Sci. Part A Polym. Chem.* **2006**, *44*, 1841–1854. [CrossRef]
75. Mani, S.; Khabaz, F.; Godbole, R.V.; Hedden, R.C.; Khare, R. Structure and Hydrogen Bonding of Water in Polyacrylate Gels: Effects of Polymer Hydrophilicity and Water Concentration. *J. Phys. Chem. B* **2015**, *119*, 15381–15393. [CrossRef] [PubMed]
76. Galanis, E.; Anderson, S.K.; Twohy, E.L.; Carrero, X.W.; Dixon, J.G.; Tran, D.D.; Jeyapalan, S.A.; Anderson, D.M.; Kaufmann, T.J.; Feathers, R.W.; et al. A phase 1 and randomized, placebo-controlled phase 2 trial of bevacizumab plus dasatinib in patients with recurrent glioblastoma: Alliance/North Central Cancer Treatment Group N0872. *Cancer* **2019**, *125*, 3790–3800. [CrossRef]
77. Gnoni, A.; Marech, I.; Silvestris, N.; Vacca, A.; Lorusso, V. Dasatinib: An anti-tumour agent via Src inhibition. *Curr. Drug Targets* **2011**, *12*, 563–578. [CrossRef]
78. Usama, S.M.; Jiang, Z.; Pflug, K.; Sitcheran, R.; Burgess, K. Conjugation of Dasatinib with MHI-148 Has a Significant Advantageous Effect in Viability Assays for Glioblastoma Cells. *ChemMedChem* **2019**, *14*, 1575–1579. [CrossRef]
79. Dumont, R.A.; Hildebrandt, I.; Su, H.; Haubner, R.; Reischl, G.; Czernin, J.G.; Mischel, P.S.; Weber, W.A. Noninvasive imaging of alphaVbeta3 function as a predictor of the antimigratory and antiproliferative effects of dasatinib. *Cancer Res.* **2009**, *69*, 3173–3179. [CrossRef]
80. de Groot, J.; Milano, V. Improving the prognosis for patients with glioblastoma: The rationale for targeting Src. *J. Neurooncol.* **2009**, *95*, 151–163. [CrossRef] [PubMed]
81. Teng, T.; Cai, Y.; Pi, W.; Gao, L.; Shay, C. Augmentation of the anticancer activity of CYT997 in human prostate cancer by inhibiting Src activity. *J. Hematol. Oncol.* **2017**, *10*, 118. [CrossRef]
82. Rice, L.; Lepler, S.; Pampo, C.; Siemann, D.W. Impact of the SRC inhibitor dasatinib on the metastatic phenotype of human prostate cancer cells. *Clin. Exp. Metastasis* **2012**, *29*, 133–142. [CrossRef]
83. Cazón, P.; Vázquez, M.; Velazquez, G. Composite films of regenerate cellulose with chitosan and polyvinyl alcohol: Evaluation of water adsorption, mechanical and optical properties. *Int. J. Biol. Macromol.* **2018**, *117*, 235–246. [CrossRef] [PubMed]
84. Mishra, S.; Bajpai, R.; Katare, R.; Bajpai, A.K. Preparation and characterization of polyvinyl alcohol based biomaterials: Water sorption and in vitro blood compatibility study. *J. Appl. Polym. Sci.* **2006**, *100*, 2402–2408. [CrossRef]
85. Lopes, J.F.A.; Simoneau, C. Solubility of Polyvinyl Alcohol in Ethanol. *EFSA Support. Publ.* **2014**, *11*, 660E. [CrossRef]
86. Schiff, D.; Sarkaria, J. Dasatinib in recurrent glioblastoma: Failure as a teacher. *Neuro-Oncology* **2015**, *17*, 910–911. [CrossRef] [PubMed]
87. Schulz, J.A.; Hartz, A.M.S.; Bauer, B. ABCB1 and ABCG2 Regulation at the Blood-Brain Barrier: Potential New Targets to Improve Brain Drug Delivery. *Pharmacol. Rev.* **2023**, *75*, 815–853. [CrossRef] [PubMed]
88. Lee, M.-J.; Lin, T.-K. Density and Viscosity for Monoethanolamine + Water, + Ethanol, and + 2-Propanol. *J. Chem. Eng.* **1995**, *40*, 336–339. [CrossRef]
89. Antoniou, E.; Alexandridis, P. Polymer conformation in mixed aqueous-polar organic solvents. *Eur. Polym. J.* **2010**, *46*, 324–335. [CrossRef]


**Disclaimer/Publisher's Note:** The statements, opinions and data contained in all publications are solely those of the individual author(s) and contributor(s) and not of MDPI and/or the editor(s). MDPI and/or the editor(s) disclaim responsibility for any injury to people or property resulting from any ideas, methods, instructions or products referred to in the content.